Feasibility of measuring magnetic resonance elastography-derived stiffness in human thoracic aorta and aortic dissection phantoms

Adnan Hirad, MD, PhD,[a] Faisal S. Fakhouri, PhD,[b] Brian Raterman, BS,[c] Ronald Lakony, BS,[a] Maxwell Wang, MD,[d] Dakota Gonring, MD,[a] Baqir Kedwai, MD,[a] Arunark Kolipaka, PhD,[c] *and* Doran Mix, MD,[a] *Rochester, NY; Riyadh, Kingdom of Saudi Arabia; Columbus, OH; and Loma Linda, CA*

ABSTRACT

Type B aortic dissection (TBAD) represents a serious medical emergency with up to a 50% associated 5-year mortality caused by thoracic aorta, dissection-associated aneurysmal (DAA) degeneration, and rupture. Unfortunately, conventional size-related diagnostic methods cannot distinguish high-risk DAAs that benefit from surgical intervention from stable DAAs. Our goal is to use DAA stiffness measured with magnetic resonance elastography (MRE) as a biomarker to distinguish high-risk DAAs from stable DAAs. This is a feasibility study using MRE to (1) fabricate human-like geometries TBAD phantoms with different stiffnesses, (2) measure stiffness in TBAD phantoms with rheometry, and (3) demonstrate the first successful application of MRE to the thoracic aorta of a human volunteer. AD phantoms with heterogenous wall stiffness demonstrated the correlation between MRE-derived stiffness and rheometric measured stiffness. A pilot scan was performed in a healthy volunteer to test the technique's feasibility in the thoracic aorta. (J Vasc Surg Cases Innov Tech 2025;11:101697.)

Keywords: Magnetic resonance elastography; Aortic biomechanics; Aortic dissection; Thoracic aortic stiffness

Type B aortic dissection (TBAD) represents a serious medical emergency with up to a 50% associated 5-year mortality.[1,2] Dissection-associated aneurysmal (DAA) degeneration and rupture cause long-term TBAD mortality, and some clinicians have advocated for early surgical intervention, but adoption of this practice has been controversial. Although some high-risk criteria imaging criteria have been shown to predict future DAA, these criteria have not been validated in clinical trials. Fundamentally, the aneurysmal dilation of the aorta derives from a mismatch between vessel biomechanical wall properties and pulsatile stresses.[3] This question, in part, can be resolved by understanding the natural history of material properties of the dissected aortic wall and its interaction with dissection-specific hemodynamics.

Although the biomechanical properties of abdominal aortic aneurysms (AAAs) have been profiled extensively, little evidence exists on the evolution of the material properties in DAA over time. AAAs usually evolve over decades, whereas DAAs may occur within a more acute period of months to years after an acute dissection. Despite this time-scale difference, we can use the extensive biomechanical evidence from AAA to guide the investigation of factors contributing to DAA. In AAA, stiffening of the aortic wall leads to pathological wall stress distribution and predisposes to aneurysmal degeneration and rupture.[4] Mechanically, increased stiffness owing to the loss of elastic lamina and increased collagen cross-linking is a significant predictor of AAA growth. In AD, the medial layer, which comprises the elastic component of the aorta, is disrupted, making the false lumen consequently stiffer.

To date, one of the greatest constraints in the study of human AD pathology is the limitation of in vivo models and their ability to reproduce the biomechanical properties of human disease. Researchers have reported various chemically induced ADs in small animal models. Unfortunately, these models have markedly different biomechanical profiles compared with human tissue[5]; therefore, new tools that directly study the human aorta are needed.

Magnetic resonance elastography (MRE) has emerged as an essential tool for imaging tissue stiffness in the liver, heart, brain, and vascular tissue.[6] In vascular tissue, MRE has been applied in AAA,[7] where aneurysm growth has been correlated with aortic wall stiffness but not aneurysmal size, the current clinical standard.[8] In MRE, tissue stiffness is based on direct measurement of micro displacements that are

From the Department of Surgery, University of Rochester School of Medicine, Rochester[a]; the Department of Biomedical Technology, College of Applied Medical Sciences, King Saud University, Riyadh[b]; the Department of Radiology, The Ohio State University, Wexner Medical Center, Columbus[c]; and the Division of Vascular Surgery, Loma Linda University Health Medical Center, Loma Linda.[d]

AH and FSF contributed equally.

Presented at the AHA Vascular Discovery: From Genes to Medicine 2023 Scientific Sessions, Boston, Massachusetts, May 10-13, 2023.

Correspondence: Doran Mix, MD, Department of Surgery, University of Rochester School of Medicine, 601 Elmwood Ave, Box 652, Rochester, NY 14642 (e-mail: dmix@urmc.rochester.edu).

The editors and reviewers of this article have no relevant financial relationships to disclose per the Journal policy that requires reviewers to decline review of any manuscript for which they may have a conflict of interest.

2468-4287

https://doi.org/10.1016/j.jvscit.2024.101697

created by externally produced mechanical shear waves.[9] Given the similarities in the biomechanical behavior of AAA and DAA, MRE could similarly be applied to AD pathology.

Although MRE has been applied to study the material properties of the abdominal aorta, and AAA, its feasibility in the thoracic aorta and DAA remains unknown. To this end, this study aims to (1) investigate stiffness contrast in hydrogel phantoms with human-like dissection geometries by using MRE and (2) demonstrate the first successful application of MRE to the thoracic aorta of a human volunteer.

METHODS

TBAD phantom fabrication. Four two-lumen TBAD phantoms were created, each comprising two different polyvinyl alcohol cryogel (PVA-c) concentrations designed to mimic hypothesized stiffness differences between the true and false lumen. The stiffness values of the phantoms fall within the range reported for human aortic tissue stiffness.[10,11] The design is based on the hypothesis that the primary stiffness contrast between the true and false lumen is driven by the characteristics of the dissected wall, which we assume is more collagenous and adventitial, and the true lumen, which likely has intact media rich in elastin. Both regions are expected to be stiffer than the dissection flap itself, meaning that the stiffness gradient primarily arises from the contrast between the true and false lumens rather than the flap. To create the model, a three-part polylactic acid phantom mold assembly, Fig 1, was printed using a Raise3D Pro2 Series desktop printer (Raise3D, Lake Forest, CA). Phantom molds were designed to mimic an AD. Each mold has two distinct lumens with total diameter of 30 mm and a total length of 200 mm. The phantom has a 5-mm vessel wall and a 3-mm-thick dissection flap, consistent with human AD geometries. In all models, the right sidewall was composed of 10% PVA to replicate the true lumen and the left sidewall would represent the false lumen with increased stiffness composed of 10% (control), 15%, 20% or 25% PVA. Three mold subassemblies—A, B, and C (Fig 1)—were required for phantom creation. Assembly A was injected with a designated concentration of 10%, 15%, 20%, or 25% by weight PVA-c to create the false lumen sidewall. Assembly A then underwent a 12-hour freeze at −20°C to solidify the PVA-c. In the next step, the frozen assembly A and an empty assembly B were assembled inside assembly C. Next, 10% PVA-c was injected into empty assembly B to create both the true lumen sidewall and the dissection flap. Assembly C prevented leakage of PVA-c and provided apposition of assemblies A and B for optimal bond cross polymerization. The assembly underwent four freeze-thaw cycles from −20°C to 20°C for PVA-c cross-polymerization. Phantoms were then stored in chlorinated 20°C water until MRE testing. All models were tested within 1 month of creation to prevent changes in the hydrogel material properties. Both MRE and rheometry experiments were conducted within 1 month of creating the phantoms to ensure the integrity of the stiffness gradient. All phantoms were stored under identical conditions, so any potential changes in stiffness during this period would likely affect all phantoms uniformly. Because the primary goal of this feasibility study was to assess relative, rather than absolute, stiffness, these conditions were sufficient for maintaining the gradient across samples.

TBAD phantom MRE image acquisition and processing. The four TBAD phantoms were scanned in a 3T-MR scanner (MAGNETOM Prisma, Siemens Healthcare, Erlangen, Germany). Each phantom was scanned individually and phantoms were positioned in a fixed position with the 10% PVA-c true lumen is always facing left and the variable 10% to 25% PVA-c false lumen facing right. The specific orientation was used to maintain consistency across experiments so true and false lumens measurement of stiffness were not mistakenly mixed during processing. A cardiac-gated spin-echo echo planar imaging (SE-EPI) sequence was used with the following parameters: 5 mm thick coronal slices, field of view (FOV) of 32 × 32 cm^2, acquisition matrix of 256 × 256, TR of 228.48 ms, TE of 11.93 ms, motion encoding gradient (MEG) frequency of 100 Hz, and mechanical frequency of 70 Hz. Mechanical vibration was introduced into both sides of the phantom using a Resoundant active driver system (Resoundant, Rochester, MN), which is connected via a tube to an in-house-designed pneumatic passive driver and phantom holder. This custom-designed system was three-dimensionally (3D) printed to enhance vibration propagation into the AD phantom. The phantom housing unit includes two rectangular windows (14 × 36 mm) (Fig 1, bottom left), which allowed the active pneumatic driver to couple vibration into the phantom via thin diaphragms. These diaphragms vibrate simultaneously upon connection to the active driver system, allowing the two walls of the phantom to get the same vibrations. Additionally, the setup positions the driver at a 90° angle relative to the phantom wall to ensure that the generated waves remain as planar as possible, optimizing wave propagation for accurate stiffness measurement.[12] The passive driver (Fig 1) was 3D printed using Stratasys's VeroClear printing material and a Stratasys Objet 750 Multi Jet 3D printer (Stratasys, Edina, MN).

Because this was a validation experiment, phantoms where tested open ended without pressurization of air or fluid within the lumens. Owing to the simplicity of the phantom structure and the presence of well-distinguished planar waves, shear stiffness was calculated manually from the wavelength of a planar propagating wave using the following equation: $\mu = \rho f^2 \lambda^2$,

Fig 1. (Top left) Shells A, B, and C, disassembled. (Top middle) Shells A, B, and C, assembled into the mold. (Top right) Cyrogel phantom removed from the mold. (Bottom left) In-house-designed and -built passive driver, with dual diaphragms to deliver vibrations to each side of the phantom separately but simultaneously. (Bottom right) Demonstration of placement of phantom on driver.

where μ is the shear stiffness, ρ tissue density, f external mechanical vibration frequency, and λ is the propagating wave wavelength. The wavelength was calculated by automated counting of the number of pixels within one cycle of full wavelength using the MRELab algorithm. Then, the number of pixels was converted to spatial displacement by multiplying the number of pixels by pixel size. Finally, the resultant was calculated in the equation as λ^2, 1000 g/cm^3 was used as ρ, and 70 Hz was used as f^2.

Fig 2. Healthy volunteer setup in which the passive driver (red arrow) is under the scapular bone and the left lateral edge of the vertebral column.

Healthy volunteer thoracic aorta MRE image acquisition and processing. The thoracic aorta of a 42-year-old healthy male volunteer was scanned with the approval of the institutional review board using the same 3T-MR scanner (MAGNETOM Prisma, Siemens Healthcare). This study primarily aimed to demonstrate the (1) parity of MRE and rheometry measured stiffness and (2) feasibility of performing an EPI-based MRE in the thoracic aorta; thus, a single healthy volunteer was sufficient. Mechanical vibration was introduced into the thoracic aorta by placing a commercially available passive driver (Resoundant) under the volunteer's left shoulder's scapular bone in the supine position (Fig 2). The same SE-EPI sequence was used with the following protocol parameters: 6 mm sagittal slices, FOV of 36 × 36 cm^2, acquisition matrix of 256 × 256, TR of 171.36 ms, TE of 11.88 ms, and 8 cardiac segments. Like the phantom scans, the MEG frequency was 100 Hz, and the mechanical frequency was 70 Hz. MEG encoding was applied in three axes, *X*, *Y*, and *Z*, to encode complex waves that would propagate in all directions. Overall, the scan in the healthy volunteer required approximately 20 minutes. This includes three slices, each collected in three mechanical encoding directions, totaling nine scans, with each scan necessitating a 10-second breath hold. Additionally, a localization sequence was conducted in three spatial directions (axial, coronal, and sagittal), followed by a candy cane sequence that allows for collection of three aortic slices in multiple orientations.

Owing to the complexity of the propagating wave within the human body and the difficulty of obtaining clear planar waves, shear stiffness was calculated using the local frequency estimation algorithm (MRElab, Mayo Clinic, Rochester, MN).[12] First, to minimize blood flow artifacts, the data were acquired in diastole. Second, the thoracic aorta was delineated by an experienced user, marking the region of interest on the magnitude image of the descending thoracic aorta. Third, an in-plane eight-direction fourth-order Butterworth band pass filter was applied to eliminate unwanted longitudinal and reflected waves with cutoff values of 1 to 40 waves per FOV.[12] Finally, 3D local frequency estimation was used to calculate a single weighted stiffness map. The stiffness map weighting was based on first harmonic amplitude for each encoding direction (*X*, *Y*, and *Z*).

TBAD phantom rheometric stiffness testing. Rheometric experiments were conducted on a TA Instruments Discover Hybrid −2 Rheometer (New Castle, DE). The 8-mm round samples were cut out of the phantom wall using a punch biopsy blade. The sample is placed on the Peltier plate. For all samples, an 8-mm geometry was lowered to achieve an axial force of 0.300 to 0.340 N with a test spacing of 1 mm and a 300-second equilibrium period. Using a previously published method, the complex shear modulus was calculated using an oscillation amplitude scan, in deformation control mode, with a strain sweep range of 0.1% to 20.0%, at a single frequency of 1 Hz, and a temperature of 25°C.[13,14]

Statistical analysis. We performed a regression model coefficient of determination (R^2) between rheometric stiffness measurements and MRE generated stiffness estimates, using GraphPad Prism version 10.0.0 for Mac (GraphPad Software, Boston, MA).

RESULTS

TBAD phantom MRE and rheological stiffness. Fig 3 displays MRE magnitude and wave images of both sides of the TBAD phantoms. Planar waves were clearly observed in the TBAD phantoms (Fig 3). The MRE SE-EPI sequence effectively generated contrasting planar waves in both the false and true lumens of the phantom in the *X* direction.

The wavelength (μ) of the 10% PVA-c side of all TBAD phantoms was 81.00 ± 0.73 mm, corresponding with 64.80 ± 2.68 pixels of size 1.25 × 1.25 mm, resulting in an MRE shear stiffness of 32.19 ± 2.66 kPa. The wavelength (μ) of the 15% PVA-c side of the TBAD phantom was 102.5 mm, corresponding with 82 pixels of size 1.25 × 1.25 mm, resulting in an MRE shear stiffness of 51.48 kPa. The wavelength (μ) of the 20% PVA-c side of the TBAD phantom was 110 mm, corresponding with 88 pixels of size 1.25 × 1.25 mm, resulting in an MRE shear stiffness of 59.29 kPa. The wavelength (μ) of the 25% PVA-c side of the TBAD phantom was 122.5 mm,

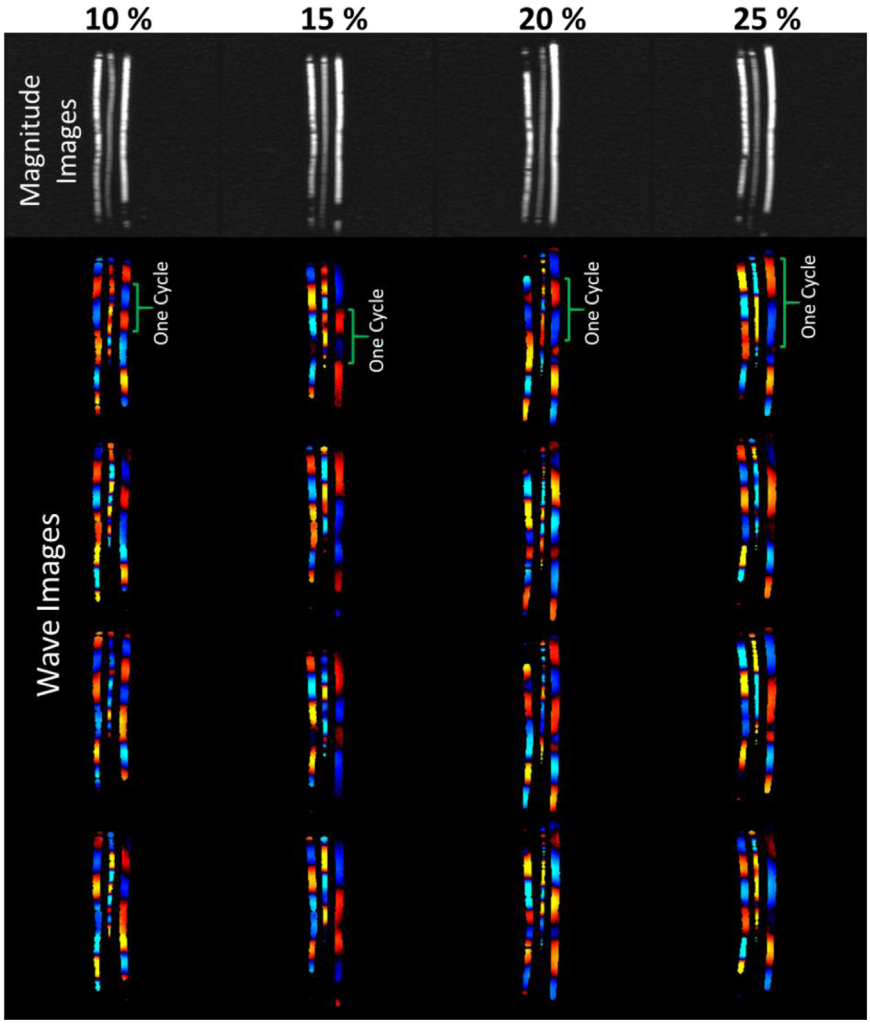

Fig 3. Magnetic resonance elastography (MRE) magnitude and wave images of each side of the type B aortic dissection (TBAD) phantoms with polyvinyl alcohol cryogel (PVA-c) concentrations of 10%, 15%, 20%, and 25%. As shown by the green curled brackets, the wavelength for a given cycle increases with increasing stiffness (ie, increasing PVA-c concentration). The column of four wave images under each PVA-c phantom represents phase offsets, capturing snapshots of displacement at four distinct time points.

corresponding with 98 pixels of size 1.25 × 1.25 mm, resulting in an MRE shear stiffness of 73.53 kPa.

Given the shear rate (frequency) difference between the two modalities (1 Hz for rheologic testing and 70 Hz for MRE) and the viscoelastic properties of the phantoms, the magnitudes of MRE and rheometric-derived stiffness are not expected to be identical. However, the expected increase in stiffness with increasing PVA-c concentration is evident in both modalities (Fig 4). Fig 4 shows the correlation ($R^2 = 0.99$) between MRE and rheometric stiffness measurements of the four phantoms with different PVA-c concentrations.

These findings demonstrate the high correlation between rheometric and MRE-generated stiffness results against an independent rheometric gold standard, highlighting the feasibility of using MRE stiffness measurements for TBAD in humans.

Healthy volunteer thoracic aorta MRE stiffness. Whereas MRE-derived stiffness measurement to stage liver fibrosis is a clinical routine, the measurement of the mechanical properties of the thoracic aorta has not been demonstrated previously because of known technical difficulties related to motion and flow artifacts by the heart and lungs.[15] Using a novel setup that delivers the mechanical vibration from the anterior side for the subject positioned in supine position, MRE data of a 42-year-old male participant was acquired successfully. Fig 5 shows the magnitude and wave images, and stiffness maps of the thoracic aorta of the healthy volunteer. The mean shear stiffness of the thoracic aorta was 3.37 ± 0.83 kPa within the aortic region of interest and is consistent with previously reported measures of healthy aortic tissue.[8,16-18] This work demonstrates the capability of performing

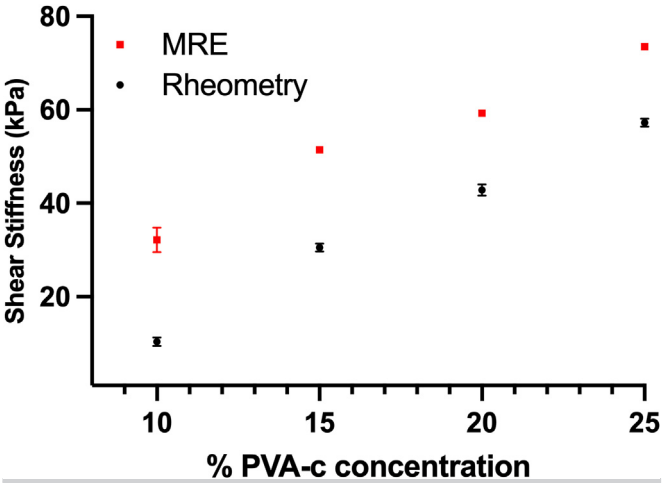

Fig 4. Correlation plot ($R^2 = 0.99$) between magnetic resonance elastography (*MRE*) and rheometric stiffness measurements of phantoms with different PVA-c concentrations of 10%, 15%, 20, and 25%. The error bars shown for the 10% PVA concentration in Fig represent the pooled data from all 10% PVA walls across the four phantoms. Because we only had one sample for each of the higher PVA concentrations (15%, 20%, and 25%), it was not possible to calculate error bars for these concentrations.

thoracic aorta shear stiffness measurement with an SE-EPI sequence with the pneumatic MRE driver system with passive driver positioned under the subject's scapular bone.

DISCUSSION

In this study, we designed and fabricated TBAD phantoms with varying PVA-c concentrations to mimic different stiffness levels in the aortic wall. Our results demonstrate that MRE can capture the stiffness variations across these phantoms effectively, as evidenced by the visualization of planar waves and contrasting stiffness measurements in the false and true lumens (Fig 3). The MRE-derived shear stiffness values for the phantoms with 10%, 15%, 20%, and 25% PVA-c concentrations showed a strong correlation ($R^2 = 0.99$) with rheometric measurements, reinforcing the reliability of MRE in capturing biomechanical properties. Furthermore, we successfully scanned and analyzed the thoracic aorta of a healthy volunteer using MRE, demonstrating the feasibility of using MRE to scan the thoracic aorta of a human subject, which is known to be challenging owing to blood flow and motion artifacts.

Distinguishing between stable dissections and DAA degeneration remains challenging and affects our understanding and management of TBAD. Although the biomechanical properties of AAA have been extensively profiled,[8,16-22] little evidence exists on the evolution of the material properties in DAA over time. In AAA, stiffening of the aortic wall leads to pathological wall stress distribution and predisposes to aneurysmal degeneration and rupture.[4] Mechanically, increased stiffness owing to loss of elastic lamina and increased collagen cross-linking is a significant predictor of aortic dilation.[23-25] In AD, the medial layer, which is the elastic component of the aorta, is disrupted[1,2,5] and is expected to make the false lumen consequently stiffer.

The expected difference in stiffness between false and true lumens informs the design of our phantom models. Increased stiffness in the false lumen contributes to increased pressures,[26] which are known to drive aneurysmal formation and degeneration through mechanisms such as wall stress,[27] inflammation, and remodeling.[28] As such, stiffness indices could become prognostic indicators for DAA formation and growth potentially change clinical decision-making regarding surgical candidates.

The successful application of MRE to measure thoracic aorta stiffness in a healthy volunteer further emphasizes its clinical potential. Prior research on AAAs has demonstrated the feasibility of quantifying aortic shear stiffness, even in the presence of blood flow and heart pulsation.[17,18] Comparisons of aortic MRE shear stiffness estimates with traditional methods, such as pulse wave velocity and four-dimensional flow,[16,19] have shown promising results. Additionally, MRE in AAA cases has revealed that stiffness measurements can provide valuable information beyond just aneurysmal diameter.[8] Consequently, MRE-derived stiffness estimates have the potential to be generalized for use in other aortic regions, including the thoracic aorta, enhancing its utility in various clinical scenarios.

This generalization is supported by studies indicating that MRE can provide valuable insights into vascular health across different aortic segments. Research has shown that MRE-derived stiffness measurements correlate well with traditional metrics like pulse wave velocity, which is recognized widely for assessing arterial stiffness.[18] Moreover, MRE offers the advantage of directly visualizing the mechanical properties of the aortic wall, providing a more localized and detailed assessment compared with global measurements like pulse wave velocity. These capabilities make MRE a promising tool for the early detection and monitoring of aortic pathologies, potentially leading to improved patient outcomes through more precise and timely interventions.

Limitations. Despite the promising results of this study, several limitations should be acknowledged. First, the TBAD phantoms used in this study, although designed to mimic different stiffness levels in the aortic wall, do not replicate the complex biological and mechanical environment of a living aorta fully. The phantoms were fabricated with varying PVA-c concentrations to simulate stiffness, but they lack the dynamic properties and intricate structure of human tissue, potentially limiting

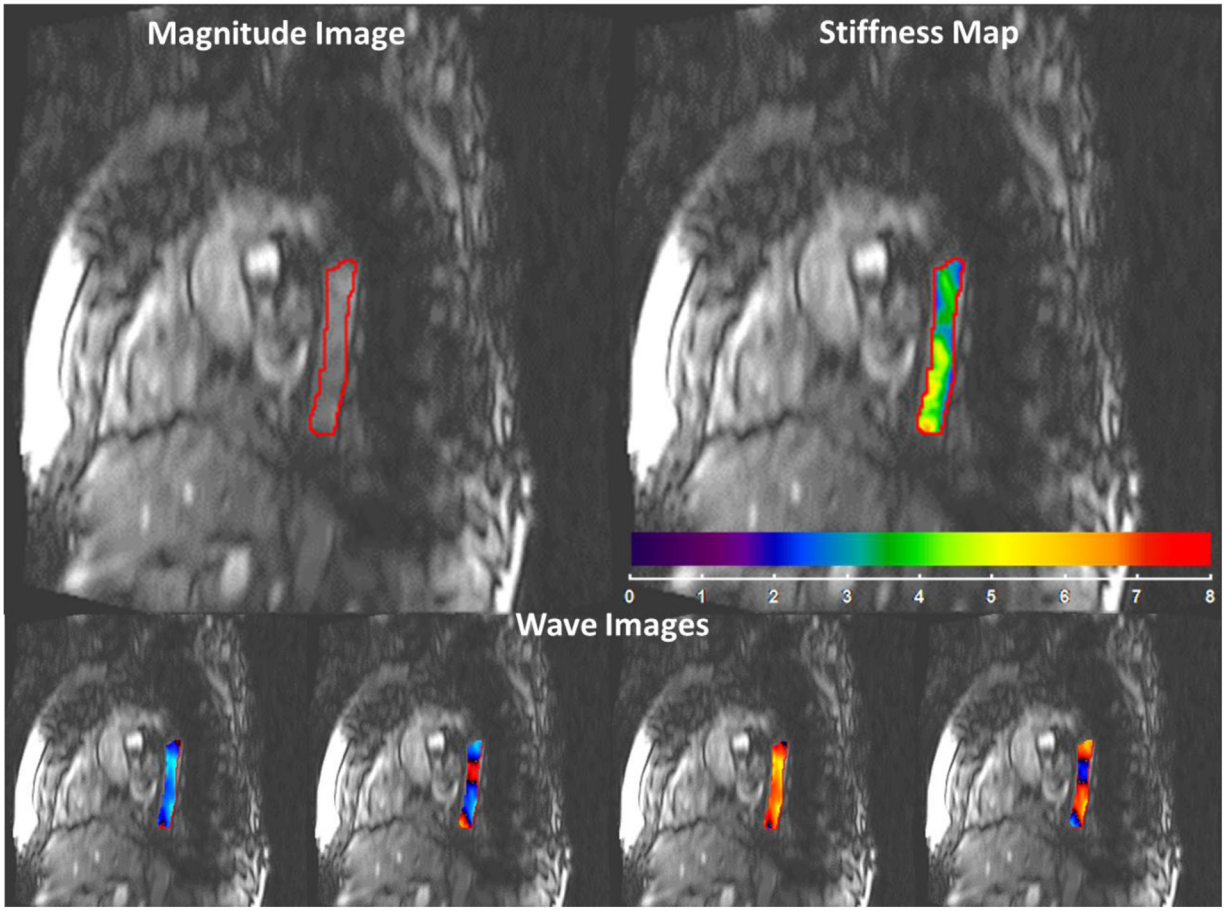

Fig 5. Magnitude image, four snap shots of wave images at different time points in read direction, and stiffness map of the thoracic aorta of a healthy volunteer with a mean shear stiffness of 3.37 ± 0.83 kPa. The row of four wave images represents phase offsets, capturing snapshots of displacement at four distinct time points.

the direct applicability of the findings to clinical scenarios. Additionally, although we successfully demonstrated the feasibility of using MRE to scan the human thoracic aorta in a healthy volunteer, blood flow and motion artifacts present significant challenges.

The study's findings on stiffness differences between false and true lumens in TBAD phantoms are based on controlled experimental conditions. Prior data have demonstrated that pressurizing a vessel can affect its material properties, including stiffness. However, because this was a validation study aiming to compare MRE-derived stiffness with the rheometric gold standard, it was critical to keep the material properties consistent with those measured in unpressurized conditions. Pressurizing the model would have introduced additional variability and altered material properties, deviating from the baseline stiffness required for accurate comparison to rheometry. In real-world clinical practice, pathophysiological variations among patients, including differences in dissection severity, aortic geometry, and individual biological responses, may influence MRE measurements. Therefore, larger studies encompassing diverse patient profiles are required to translate these findings comprehensively. Orientations of the vessel in vivo may also affect stiffness measures, especially with the additional complexity of blood flow and pulsatile pressures; as such, we will address those issues in future studies involving patients.

Finally, sample size is a limitation of our study. The successful application of MRE in thoracic aorta was demonstrated in only one healthy volunteer. We anticipate several factors will influence the validity of aortic stiffness measurements in human subjects using MRE. First, it is established that vessel pressurization impacts measured stiffness. In future studies, we plan to measure and normalize blood pressure to account for pressure-induced stiffness changes. Additionally, we will ensure data collection occurs at the same point in the cardiac cycle—specifically, diastole—to decrease pressure variability, because stiffness measures can vary by up to 27% between systole and diastole. Second, in vivo conditions often involve entry tears and fenestrations that may

create different pressures in the true and false lumens. We collected data during diastole to minimize pressure differences; however, based on available data, we expect significant inherent differences in stiffness between normal and aneurysmal tissue or between true and false lumens that remain detectable despite these variations. Third, human aortic tissue is highly heterogeneous, and future measurements will represent a regional accumulation of tissue stiffness. Although it remains unknown if this heterogeneity might limit clinical utility, we believe the differences between true and false lumen stiffness fall within a range that should allow for meaningful distinction. Fourth, owing to the complex geometry of human ADs, localization may require assumptions to identify specific aortic regions accurately. However, we expect this challenge to have minimal impact on the ability to assess gross properties of the true lumen. Prior MRE studies have distinguished between normal and aneurysmal tissue successfully, which suggests feasibility in capturing meaningful data in more complex anatomical settings. Fifth, the current analysis assumes flowing blood is incompressible and behaves similarly to adjacent vessel tissue, facilitating wave propagation through a waveguide effect. However, thrombus behaves more like soft tissue than fluid, which would likely create a stiffness contrast between the thrombus and the aortic wall. We expect this difference to affect shear wave propagation, potentially providing a distinct signal that could differentiate between thrombus-laden and nonthrombus sections of the false lumen. Finally, our current analysis, consistent with prevailing approaches in the field, assumes that flowing blood is incompressible and behaves similarly to adjacent vessel tissue, facilitating wave propagation through a waveguide effect. Under this assumption, diameter alone does not impact the MRE signal directly. However, we hypothesize that there may be a nonlinear correlation between aortic diameter and stiffness, with stiffening driving further aortic growth. At more advanced stages, this stiffness may decrease eventually, leading to conditions that predispose the vessel to rupture. To tease out these factors, studies with more extensive and diverse subject populations are essential to establish the clinical usefulness of MRE in assessing thoracic aorta stiffness. Including a broader range of participants, such as those with different stages of aortic diseases (eg, patients with chronic AD) and varying demographic characteristics, will provide more robust data and help to validate the findings across a broader spectrum of clinical scenarios.

CONCLUSIONS

This study demonstrates excellent agreement between stiffness measurements obtained using MRE and rheometry in TBAD phantoms. In addition, a feasibility study was performed in a healthy volunteer to determine the stiffness of thoracic aorta despite of heart and lung motion. We also present a method for the novel manufacturing of hydrogel AD phantoms with programmatic regional stiffness variations measured using MRE and validated against Rheometric measurements.

FUNDING

None.

DISCLOSURES

None.

REFERENCES

1. Sigman MM, Palmer OP, Ham SW, Cunningham M, Weaver FA. Aortic morphologic findings after thoracic endovascular aortic repair for type B aortic dissection. *JAMA Surg*. 2014;149:977–983.
2. Sultan I, Siki MA, Bavaria JE, et al. Predicting distal aortic remodeling after endovascular repair for chronic DeBakey III aortic dissection. *Ann Thorac Surg*. 2018;105:1691–1696.
3. Prokop EK, Palmer RF, Wheat MW Jr. Hydrodynamic forces in dissecting aneurysms. In-vitro studies in a Tygon model and in dog aortas. *Circ Res*. 1970;27:121–127.
4. Vorp DA, Vande Geest JP. Biomechanical determinants of abdominal aortic aneurysm rupture. *Arterioscler Thromb Vasc Biol*. 2005;25:1558–1566.
5. Jiang DS, Yi X, Zhu XH, Wei X. Experimental in vivo and ex vivo models for the study of human aortic dissection: promises and challenges. *Am J Transl Res*. 2016;8:5125–5140.
6. Eaton JE, Sen A, Hoodeshenas S, et al. Changes in liver stiffness, measured by magnetic resonance elastography, associated with hepatic decompensation in patients with primary sclerosing cholangitis. *Clin Gastroenterol Hepatol*. 2020;18:1576–1583.e1.
7. Khan S, Fakhouri F, Majeed W, Kolipaka A. Cardiovascular magnetic resonance elastography: a review. *NMR Biomed*. 2018;31:e3853.
8. Kolipaka A, Illapani VS, Kenyhercz W, et al. Quantification of abdominal aortic aneurysm stiffness using magnetic resonance elastography and its comparison to aneurysm diameter. *J Vasc Surg*. 2016;64:966–974.
9. Venkatesh SK, Yin M, Ehman RL. Magnetic resonance elastography of liver: technique, analysis, and clinical applications. *J Magn Reson Imaging*. 2013;37:544–555.
10. Vande Geest JP, Sacks MS, Vorp DA. The effects of aneurysm on the biaxial mechanical behavior of human abdominal aorta. *J Biomech*. 2006;39:1324–1334.
11. Humphrey JD, Holzapfel GA. Mechanics, mechanobiology, and modeling of human abdominal aorta and aneurysms. *J Biomech*. 2012;45:805–814.
12. Cai W, Wang H, Huang W, et al. Performance evaluation of a prototype pneumatic driver for MR elastography by MR elastography. Accessed December 23, 2024. https://doi.org/10.1109/BMEI.2011.6098350.
13. Guo K, Zhu Y, Wang J, Jiang C, Yu J. Characterizing the viscoelastic properties of a tissue mimicking phantom for ultrasound elasticity imaging studies. *IOP Conf Ser Mater Sci Eng*. 2019;490:022035.
14. Zuidema JM, Rivet CJ, Gilbert RJ, Morrison FA. A protocol for rheological characterization of hydrogels for tissue engineering strategies. *J Biomed Mater Res B Appl Biomater*. 2014;102:1063–1073.
15. Alfudhili K, Masci PG, Delacoste J, et al. Current artefacts in cardiac and chest magnetic resonance imaging: tips and tricks. *Br J Radiol*. 2016;89:20150987.
16. Kolipaka A, Illapani VS, Kalra P, et al. Quantification and comparison of 4D-flow MRI-derived wall shear stress and MRE-derived wall stiffness of the abdominal aorta. *J Magn Reson Imaging*. 2017;45:771–778.
17. Dong H, Jin N, Kannengiesser S, Raterman B, White RD, Kolipaka A. Magnetic resonance elastography for estimating in vivo stiffness of the abdominal aorta using cardiac-gated spin-echo echo-planar imaging: a feasibility study. *NMR Biomed*. 2021;34:e4420.
18. Damughatla AR, Raterman B, Sharkey-Toppen T, et al. Quantification of aortic stiffness using MR elastography and its comparison to MRI-based pulse wave velocity. *J Magn Reson Imag*. 2015;41:44–51.
19. Kenyhercz WE, Raterman B, Illapani VS, et al. Quantification of aortic stiffness using magnetic resonance elastography: measurement

reproducibility, pulse wave velocity comparison, changes over cardiac cycle, and relationship with age. *Magn Reson Med*. 2016;75:1920–1926.
20. van Disseldorp EMJ, Petterson NJ, van de Vosse FN, van Sambeek M, Lopata RGP. Quantification of aortic stiffness and wall stress in healthy volunteers and abdominal aortic aneurysm patients using time-resolved 3D ultrasound: a comparison study. *Eur Heart J Cardiovasc Imaging*. 2019;20:185–191.
21. Zhang N, Chen J, Yin M, Glaser KJ, Xu L, Ehman RL. Quantification of regional aortic stiffness using MR elastography: a phantom and ex-vivo porcine aorta study. *Magn Reson Imaging*. 2016;34:91–96.
22. Dong H, Mazumder R, Illapani VSP, Mo X, White RD, Kolipaka A. In vivo quantification of aortic stiffness using MR elastography in hypertensive porcine model. *Magn Reson Med*. 2017;78:2315–2321.
23. Nollen GJ, Groenink M, Tijssen JGP, van der Wall EE, Mulder BJM. Aortic stiffness and diameter predict progressive aortic dilatation in patients with Marfan syndrome. *Eur Heart J*. 2004;25:1146–1152.
24. Zottola ZR, Kong DS, Medhekar AN, et al. Intermediate pressure-normalized principal wall strain values are associated with increased abdominal aortic aneurysmal growth rates. *Front Cardiovasc Med*. 2023;10:1232844.
25. Niestrawska JA, Regitnig P, Viertler C, Cohnert TU, Babu AR, Holzapfel GA. The role of tissue remodeling in mechanics and pathogenesis of abdominal aortic aneurysms. *Acta Biomater*. 2019;88:149–161.
26. Rudenick PA, Segers P, Pineda V, et al. False lumen flow patterns and their relation with morphological and biomechanical characteristics of chronic aortic dissections. Computational model compared with magnetic resonance imaging measurements. *PLoS One*. 2017;12:e0170888.
27. Kobeissi E, Hibino M, Pan H, Aune D. Blood pressure, hypertension and the risk of abdominal aortic aneurysms: a systematic review and meta-analysis of cohort studies. *Eur J Epidemiol*. 2019;34:547–555.
28. Kessler V, Klopf J, Eilenberg W, Neumayer C, Brostjan C. AAA revisited: a comprehensive review of risk factors, management, and hallmarks of pathogenesis. *Biomedicines*. 2022;10:94.

Submitted Oct 9, 2024; accepted Nov 20, 2024.